Design and feasibility analysis of a graded harvesting end-effector with the function of soluble solid content estimation

Yufei Lin[1,2], Hao Liang[3], Junhua Tong[1], Haoyu Shen[1], Xiaping Fu[1*], Chuanyu Wu[4*]

(1. *College of Mechanical Engineering, Zhejiang Sci-Tech University, Hangzhou 310018, China*;
2. *Department of Agriculture and Biotechnology, Wenzhou Vocational College of Science and Technology, Wenzhou 325006, Zhejiang, China*;
3. *College of Mathematics and Computer Science, Zhejiang A&F University, Hangzhou 311300, China*;
4. *Zhejiang Ocean University, Zhoushan 316002, Zhejiang, China*)

Abstract: In response to the prevailing scarcity of labor and with the aim of augmenting the proportion of premium-quality fruits, a robotic grading end-effector system for harvesting was meticulously designed. The end-effector could measure the soluble solid content (SSC) of peaches during the harvesting process to evaluate the quality of the fruit, thereby facilitating real-time grading during harvesting. As comprising a harvesting component and an information-gathering segment, the end-effector system was optimized with the primary structural parameters of its adaptive fingers using a mathematical model of peach morphology. Also, the buffering materials for mitigating the pressure exerted by the adaptive fingers on the peaches were compared. Furthermore, feasibility analyses of the grasping actions were conducted based on the interaction forces between the adaptive fingers and the peaches. To grade the quality of peaches, SSC was used as an indicator to assess and grade the quality of the peaches. The spectra of peaches within the wavelength range of 590-1100 nm were collected, and a predictive model for SSC was developed. The correlation coefficients for the calibration set and prediction sets of the predictive model were 0.880 and 0.890, with corresponding root mean square errors of 0.370% and 0.357% Brix, respectively. In addition, a robustness and accuracy assessment was conducted using 30 peach samples, yielding a correlation coefficient of 0.936 and a standard error of 0.386% Brix between the predicted and measured values of SSC. The results confirm that the end-effector can measure the SSC of peaches during the collection process, providing novel concepts and theoretical foundations for real-time harvesting and grading.

Keywords: robot harvesting, graded end-effector, soluble solids, near-infrared spectroscopy

DOI: 10.25165/j.ijabe.20241705.7901

1 Introduction

Peach is a popular fruit owing to its high nutritional value and excellent taste. However, because of their high moisture contents, peaches are prone to browning, softening, and rotting, particularly when they are damaged during harvesting and transportation[1]. The harvest time of peaches is extremely short, about 15-30 d for one variety. If they cannot be harvested in time, the fruit will fall off, resulting in a waste of resources and pecuniary losses[2]. The labor required for fruit harvesting accounts for about 40% of the labor required in the entire production process[3]. High labor intensity, intensive operation times, and labor shortages have been identified as factors restricting fruit production. The development of

harvesting robots is conducive to the alleviation of the above problems and reduction of the fruit production costs[4].

As a key component of robot harvesting, the end-effector has attracted the attention of many researchers[5-9]. The primary function of the end-effector is to grasp the fruit, effectuate its detachment from the fruit stem, and subsequently position it within a designated collection area. There are two main methods for fruit harvesting[10]. The first method involves grasping and cutting. After the end-effector grabs the fruit, a cutter, such as scissors, blades, or saws, cuts the stalk[11,12]. This method is widely employed, particularly for fruits with high binding forces with fruit stalks, such as cucumbers[13,14]. However, determining the accurate cutting positions of fruit stalks and avoiding damage to other branches and vines of crops is difficult[15]. Furthermore, this method requires a high-accuracy end-effector. Xiong et al.[16] designed a strawberry harvesting end-effector that could effectively avoid the damage caused by grasping. Furthermore, Xu et al.[17] designed a navel orange harvesting end-effector, which uses underactuated double V-shaped fingers to realize harvesting and simplify the control system. The second method is bionic harvesting. The end-effector separates the fruit and fruit stalk after grasping the fruit via screwing, folding, and pulling. It is suitable for cutting the fragile connection between the fruit and the fruit stalk. However, this method requires an end-effector that realizes multiple-degree-of-freedom motion, multidimensional control, and large torques. The end-effector developed by Mu et al.[18], which is equipped with bionic fingers and

automated mechanisms, approaches kiwifruit from below, using a trajectory model validated through the ADAMS software (MSC, USA) simulation. This integrated system, featuring fiber and pressure sensors in a prototype, effectively separates and grabs individual fruits, demonstrating the potential for streamlined kiwifruit harvesting. The above end-effectors were designed according to the characteristics of the harvesting object and are only suitable for harvesting one target. Thus, it is imperative to develop a universal harvesting terminal for specific types of fruit to improve the use of the harvesting execution terminal.

The adaptive robotic finger was derived from the MultiChoice Gripper product manufactured by FESTO® utilizing the flexion capability inspired by bionic fins[19]. When the inner surface of the finger is subjected to pressure from the grasped object, the finger bends in the opposite direction of the thrust and generates a reverse force. The reverse force is then distributed along the outer contour of the grasped object and envelops the outer contour to achieve the clamping effect. The adaptive finger can perform different degrees of bending based on the different shapes of the clamped object, thus having advantages such as simple structure, compactness, and good clamping performance. This adaptive clamping mechanism only requires one stepping motor as the power input. The use of this adaptive finger as the clamping mechanism of the end-effector not only realizes high flexibility and good interactions but also reduces the complexity of control.

Fruit quality is important for consumers, and it has become a requirement for suppliers to provide fruits with high-standard quality[20]. At present, fruit grading mainly depends on manual operation. Some large farms use grading lines to grade fruits after the harvesting process. Most of the fruit classifications are based on the appearance quality[21-23]. However, manual grading standards are not unified and have low accuracy and efficiency[23]. The use of grading lines increases the potential for mechanical damage, particularly for thin-skinned and soft fleshy fruits, such as peaches[24]. It effectively reduces the mechanical damage rate of soft fruits during the harvesting process.

Dewi et al.[25] introduced a 4DOF fruit-sorting robot that uses image processing based on HSV analysis for color recognition and grayscale analysis for diameter determination. It demonstrates effectiveness in sorting red and green tomatoes as well as red and green grapes within a packaging system. A winter jujube grading robot that uses a method integrating the YOLOv3 algorithm and hand-engineered features was designed to categorize mature winter jujubes based on their red color[26]. The aforementioned research only conducted the grading operation based on the external quality of the fruit; however, the internal quality is also an important index for fruit evaluation. Near-infrared spectroscopy (NIRS) can predict the internal quality of fruit nondestructively, efficiently, and quickly, and it can meet the requirements of onsite detection[27-29]. It has played a pivotal role in improving the automation level of fruit production. The miniaturization and portability of NIR spectrometers make it possible to apply NIR nondestructive testing technology in fruit harvesting[30].

Aiming at soft spherical fruits that are not suitable for online grading, this study explores the grading process during robot harvesting. There are two main challenges in graded harvesting. One is that the end-effector can easily damage the fruit, and the other is the basis for fruit grading. Therefore, this study aimed to design an end-effector for the graded harvesting of soft fruits and to explore the feasibility of taking the internal quality as a grading index in the graded harvesting process.

2   Materials and methods

2.1   End-effector system

2.1.1   Structure of the end-effector system

As shown in Figure 1, the structure of the graded harvesting end-effector was mainly composed of a connecting bracket, control unit, clamping mechanism, and spectrum acquisition unit. The detailed components are shown in Figure 1. The main function of the end-effector system is to harvest and grade fruits. Harvesting mainly depends on the clamping mechanism to clamp and separate fruits. The gradation is mainly based on the spectrum collected by the light probe, and the internal quality is predicted based on the spectrum. The clamping mechanism is the major component of the end-effector, which is controlled by a stepper motor. The more degrees of freedom the harvesting fingers have, the more flexible the grasping action and the better the grasping effect is; however, the complexity, cost, and control difficulty of the system also increase.
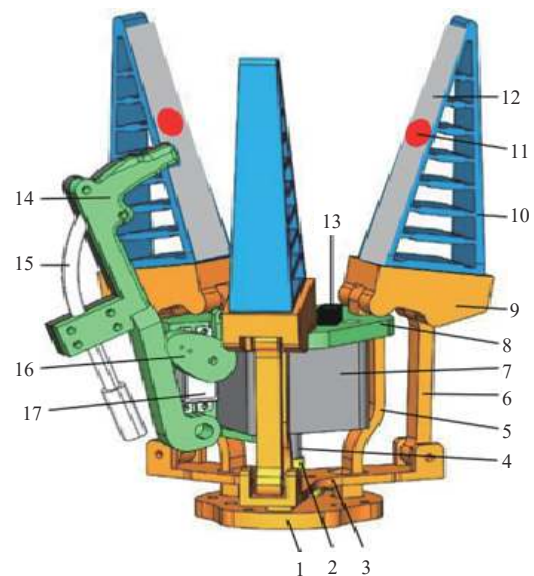
1. Connecting bracket, 2. Coupling, 3. Thrusters, 4. Ball screw, 5. Bracket, 6. Connecting rod, 7. Stepper motor, 8. Fixed base, 9. Finger base, 10. Adaptive finger, 11. Thin-film pressure transducer, 12. Buffer material, 13. Infrared proximity switch, 14. Fiber optic connecting rod, 15. Fiber optic, 16. Cam, 17. Steering engine

Figure 1   Structure diagram of end-effector

Another major component is the spectral data acquisition system. To facilitate the operation, a fiber optical probe was placed on the end-effector. The distance and proximity between the fiber optical probe collecting spectral data and the fruit were controlled by the steering gear. The spectrum acquisition system required the fiber optical probe to come into contact with the target peach to collect the spectrum. After the collection, the fiber optical probe was separated from the target peach. To achieve the above requirements, a fiber optical fixed connecting rod was designed for pulling the fiber optical probe. The steering gear was used as the power input. The steering gear drove the cam to rotate so as to achieve contact and separation between the fiber optical probe and the target peach. The Y-type fiber optical was connected to a spectrometer and a light source to complete the spectrum acquisition of the target peach.

2.1.2   Components of the end-effector system

The schematic of the end-effector system is shown in Figure 2.

The system is composed of an end-effector, spectrometer, light source, controller, computer, and signal transmission. To obtain a robust spectral signal, a Y-type fiber optical was used to connect the spectrometer to the light source. A Bluetooth signal transmission between the computer and the controller could facilitate the harvesting operation and data acquisition. The control software interface was used to control all the operations of the harvesting process.
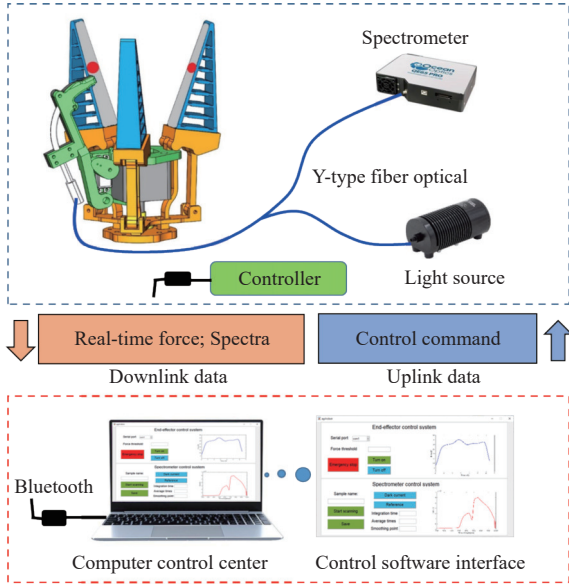

Figure 2　Schematic of the end-effector system and control software

The end-effector adjusted position based on the position of the target fruit monitored by the infrared switch to complete the positioning and reach the preset harvesting distance. After the positioning, the electromagnetic relay sent a pulse signal to the single-chip microcomputer. The single-chip microcomputer sent feedback to the two components of the end-effector: the clamping mechanism and the spectrum acquisition unit. The stepping motor drove the thrusters to move forward through a ball screw to push the connecting rod, which pushed the finger base to rotate around the hinge. The fingers were closed and bent until they fit the fruit surface to clamp the fruit. When the positive pressure on the membrane pressure sensor on the finger surface reached the set safety threshold, the stepping motor stopped working. During this time, the steering engine drove the fiber optic connecting rod close to the target peach, and then the fiber optical probe collected the spectrum of the peach. After the spectrum data were transmitted to the computer, the soluble solid content (SSC) of the peach was predicted by a pre-established model. The host computer graded the peach through the SSC and transmitted the information to a single-chip microcomputer to control the harvesting end-effector to reach the specified position. The end-effector released the fruit and completed the harvesting action.

2.2　Force analysis between the peach and the end-effector

To prevent mechanical damage to the peaches by the adaptive fingers during the harvesting process, an analysis of the interactive forces between the two was conducted, along with the determination of the mechanical damage threshold for the peaches.

2.2.1　Measurement of physical parameters of samples

After being harvested by the end-effector system, the peaches were transported to the laboratory for measurement. The heights and two diameters of the peaches were measured using vernier calipers to obtain the fruit shape indices. It is noteworthy that in the measurement process, the two diameter values refer to the dimensions along the x and y axes defined in Figure 3. The calculation equations[31] of the other parameters are as follows:

$$d_g = (hd_1d_2)^{\frac{1}{3}} \tag{1}$$

$$\Phi = d_g/h \tag{2}$$

where, d_g denotes the fluid density, h is the height of the peach (the z-axis direction of Figure 3), d_1 is the transverse diameter (the x-axis direction of Figure 3), d_2 is perpendicular to d_1 (the y-axis direction of Figure 3), and Φ is the sphericity. The peach masses were obtained using a balance with an accuracy of 0.01 g. For the convenience of mechanical analysis, the mass was converted into a gravitational force, i.e., the weight.
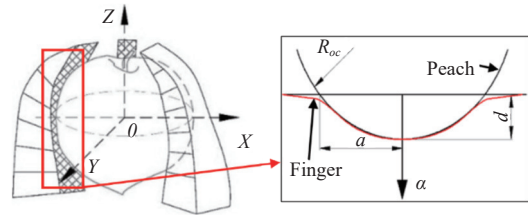

Figure 3　Mathematical model and force analysis of peach

2.2.2　Theoretical analysis of the force interaction between the fingers and the peaches

To safeguard against mechanical damage during the harvesting process, the force exerted by each finger on the peaches was analyzed. The finger surface was flat when it was in its natural state. Assuming the contact surface of the peach does not deform, as shown in Figure 3, the bending deformation of the finger caused because of contact with the peach can be regarded as the deformation resulting from an elastic plane coming into contact with a rigid sphere. The contact between a single finger and a peach is shown in Figure 3. If the normal displacement of a point on the surface of the elastic surface is u_α, and d denotes the maximum bending distance; a is the contact radius; R_{oc} is the radius of curvature of the contact circle; If the normal displacement of a point on the surface of the elastic surface is u_α, α represents the normal vector of the point of contact between the finger and the peach, then[32]:

$$u_\alpha = d - \frac{a^2}{2R_{oc}} \tag{3}$$

The distribution of the force $p(r)$ acting on the elastic plane is as follows[32]:

$$p(r) = P_0\sqrt{1 - \frac{r^2}{a^2}} \tag{4}$$

where, P_0 denotes the intermediate variable of the force, and r denotes the intermediate variable of the contact radius.

The resulting normal displacement is[32]:

$$u_\alpha = \frac{\pi P_0}{4E^*a}(2a^2 - r^2) \tag{5}$$

where, E^* denotes the elastic modulus. Thus,

$$a = \frac{\pi P_0 R_{oc}}{2E^*} \tag{6}$$

$$d = \frac{\pi a P_0}{2E^*} \tag{7}$$

$$a^2 = R_{oc}d \tag{8}$$

$$P_0 = \frac{2}{\pi} E^* \left(\frac{d}{R_{oc}} \right)^{\frac{1}{2}} \tag{9}$$

The resultant force of the whole peach from one finger is as follows:

$$F = \int_0^a p(r) 2\pi r \mathrm{d}r = \frac{2}{3} P_0 \pi a^2 = \frac{4}{3} E^* d (Rd)^{\frac{1}{2}} \tag{10}$$

$$d = R_{oc} \left[1 - \cos \left(\frac{180l}{2\pi R_{oc}} \right) \right] \tag{11}$$

where, l denotes the effective length of the finger. Thus,

$$F = \frac{4}{3} E^* R_{oc}^2 \left[1 - \cos \left(\frac{180l}{2\pi R_{oc}} \right) \right]^{\frac{3}{2}} \tag{12}$$

It can be seen from Equation (12) that with a certain mass, properly increasing the static friction coefficient can reduce the pressure of the fingers on the peach. Because adaptive fingers need to bear the weight of the peach, there are requirements for the strength of the finger materials.

2.2.3   Experimental investigation of the force interaction between the fingers and the peaches

Therefore, to increase the static friction coefficient when the finger surface comes into contact with the peach and to reduce the damage to the peach, the inner finger surface was covered with a layer of buffer material[33]. There are three common cushioning materials: rubber, silica gel, and pearl cotton. Friction tests between the peach skin and the aforementioned cushioning materials were conducted using an MXD-2 friction coefficient tester (Labthink, China) to determine the material with the greatest static friction coefficient. The test speed was 100 and 150 mm/min (two loading speeds of friction coefficient measuring instruments), and each friction material was subjected to 20 repeated tests under 100 and 200 g of loading.

2.2.4   Compression tests on peaches at varying ripeness stages

For the sake of convenient storage and transportation in actual production, peaches are often harvested during the green ripening period. For local sales and processing, harvesting during the half-ripe periods can be chosen. To compare the loading capacities of peaches at different ripeness stages, 20 peaches each from the green, green-ripe, semi-ripe, and fully ripe stages were selected for compression characteristic tests, with the horizontal and vertical diameters of the peaches ranging from 56.2 to 91.5 mm and 53.8 to 78.5 mm, respectively. The experiments were conducted on the microcomputer-controlled electronic universal testing machine of WDW30001 (YDYQ, China), with a force sensor range of 1000 N, accuracy of 0.5%, and resolution of ±1/240 000. The loading and unloading were automatically controlled by the computer, and data acquisition was automatically performed. A cylindrical indenter with a 7.9 mm was used as the loading tool in the experiment, with the loading rate set to 0.25 mm/s.

2.3   Detection of the intrinsic quality of peaches

Figure 4 shows the procedural intricacies involved in the noninvasive determination of the internal quality of peaches during the harvesting phase. Initially, samples were arbitrarily chosen from the orchard, and their spectra were obtained. Subsequently, these specimens were transported back to the laboratory for the determination of their SSC. Using the collected spectra and their corresponding chemical values, a predictive model for chemical composition was developed.
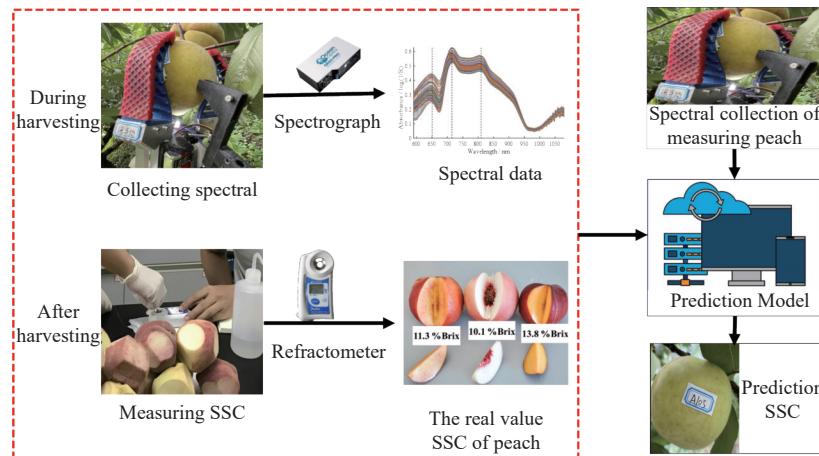

Figure 4   Process of establishing a peach prediction model and predicting soluble solid content (SSC)

The aforementioned method for measuring internal quality, seamlessly integrated into the harvesting endeavor, concurrently achieves the discernment of the specimens' intrinsic quality.

2.3.1   Peach sample preparation

The test was conducted in an orchard in Yuhang District, Hangzhou in July 2021, and the test samples were honey peaches. To simplify the test, the end-effector was fixed using a height-adjustable tripod instead of a mechanical arm. Because this study did not involve visual recognition, the position of the fruit was assumed to be known. The center of the fruit was placed with the central symmetry of the end-effector on the same line, and the test was conducted using the control system of the end-effector.

In the test, a sample fruit was randomly selected, with two or three on each fruit tree, and numbered. Then, spectral data was collected during harvesting. After harvesting, 135 samples without damage and defects were chosen and transported to the laboratory to complete the physicochemical property measurements and spectral acquisition within 4 h.

2.3.2   Spectral data collection of the samples

The spectra of the peach samples were obtained onsite during the harvesting process using the end-effector execution system. The NIR spectrum for the fruit internal quality estimation was concentrated between 700 and 900 nm[34]. A spectrometer (Ocean Insight, QE65Pro, USA) with a wavelength range of 200-1100 nm and a resolution of 0.8 nm, with a 20 W halide tungsten lamp (Ocean Insight, HL-2000-HP, USA) as the light source was used to build the spectrum acquisition unit.

This spectrometer could predict the internal quality of fruits

and vegetables. Considering the spatial layout of the device, the reflected light measurement was adopted. Considering that the external ambient light was unstable in the harvesting field operation, a Y-type fiber optical was designed to detect the end-effector signal and the light source together to simplify the structure of the end-effector. To complete the spectral information collection, the light emitted by the light source was reflected by the measured object and transmitted into the spectrometer through the fiber optical. A shading rubber pad could be attached to the sample surface based on the shape of the sample to prevent light overflow and reduce the error caused by the differences in the sample shapes.

2.3.3　Measurement of SSC in the samples

The SSCs of the peaches were measured using a PAL-1 hand-held refractometer (ATAGO, Japan). The instrument parameters were as follows: measurement range, of 0% Brix-53.0% Brix; measurement temperature, 1°C-75°C (automatic temperature compensation); sample size, 0.3 mL; and measurement time, 3 s. The SSC of each peach was measured via sampling according to the standard method. At the corresponding spectral acquisition point, about 1 cm³ of the peach pulp was taken after peeling to squeeze its juice and drop it on the handheld refractometer for measurement. The average value of the six measurements was taken as the SSC of the peach.

2.3.4　Spectral data preprocessing method

The spectral data at the wavelength of 590-1100 nm was selected for the preprocessing and modeling. The spectrometer was used to collect the light intensity information. First, the light intensity signal was transformed into a reflection spectrum. The reflectivity calculation equation is as follows:

$$R = \frac{I_s - I_b}{I_r - I_b} \times 100\% \tag{13}$$

where, R denotes the reflectivity of the peach sample, I_s is the spectral intensity reflected by the peach, I_r is the spectral intensity reflected by the standard whiteboard, and I_b is the dark current.

To establish a robust prediction model, the reflectance should be further converted into the absorbance according to the Beer-Lambert law. The conversion equation is as follows:

$$A = -\log(1/R) \tag{14}$$

where, A denotes the absorbance of the sample, and R denotes the reflectivity of the peach sample.

In addition to the information on the test samples, the collected visible and NIR spectra often contained interference noise independent of the properties of the samples to be tested. Due to the influence of environmental factors, such as stray light and the dark current of the instrument itself, the original spectral data needed to be preprocessed first. Savitzky-Golay smoothing (SGS) was employed to reduce the random error and improve the signal-to-noise ratio by averaging the spectral information data many times. The Savitzky-Golay derivative (SGD) was used to eliminate the interference caused by baseline drift or the flat background by differentiation, to distinguish overlapping peaks, and to improve resolution and sensitivity. Multiplicative scatter correction (MSC) could effectively eliminate the spectral differences caused by different scattering levels to enhance the correlation between the spectra and data. The transformation of the standard normal variate (SNV) was mainly used to eliminate the effects of the solid particle size, surface scattering, and optical path change on the visible and NIR diffuse scattering spectra. It is extremely important to select a suitable pretreatment method to weaken this interference and ensure

the accuracy of the calibration model.

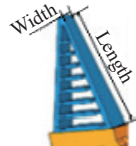### 2.3.5　Partial least squares regression (PLSR) model for predicting SSC

As a mature linear multivariate correction method, PLSR has been widely used in NIRS. The quantitative relationship between the spectra and the SSCs of the peaches was established via PLSR, and the prediction accuracy of the model was tested using an independent validation set. The samples were randomly divided into a calibration set and a validation set at a 3:1 ratio. The determination coefficient of calibration (R_c^2), determination coefficient of validation (R_v^2), root mean square error of calibration (RMSEC), and root mean square error of validation (RMSECV) were utilized to evaluate the modeling effect. Higher values of R_c^2 and R_v^2 and smaller values of RMSEC and RMSECV corresponded to a more robust predictive model, but there was a small difference between RMSEC and RMSECV.

3　Results and discussion

3.1　Parameters of end-effectors

The agricultural industry standard of the People's Republic of China (NY/T 586-2002) specifies that the range of peach diameters should be 52-80 mm and the maximum weight of a single fruit should be 230 g. To increase the range of fruit harvesting, the finger length was increased by 25% based on the diameter, and the finger length was 100 mm as listed in Table 1. The maximum diameter of the extended finger was determined to be 120 mm, and the three fingers were arranged at 120° when the finger base was 20 mm. The minimum diameter of the formation space was 40 mm when the finger closed and the maximum value was 135 mm when the finger opened. Hence, such a dimensioned design entirely caters to the harvesting of diverse peach varieties and meets the harvesting requirements for other spherical fruits.

Table 1　Specifications of the main components of the end-effector

Component name	Object pictures	Specifications
Finger		Length: 100 mm, Width: 16 mm
Finger distribution		Uniform distribution 120°
Thin film pressure Sensor		Diameter: 15.0 mm, Thickness: 0.4 mm
Fiber optic probe		Diameter: 4 mm

The coefficients of friction between the different buffering materials and the peach skin are presented in Table 2. The coefficient of friction for silica gel is markedly higher than that of the other two materials. Consequently, silica gel was selected as the

surface buffering material for the fingertips of the end-effector. In addition, both the loading speed and positive pressure influenced the coefficient of friction. Specifically, a higher loading speed results in a smaller coefficient of friction. This is attributed to the fact that with a faster loading speed, the contact pressure on the peach surface increases. Under the condition of constant instantaneous frictional force, a higher loading speed leads to a smaller coefficient of friction. Conversely, a greater load mass corresponds to a larger coefficient of friction. To determine the maximum positive pressure at the contact between the fingertip and the peach, a scenario with a smaller coefficient of friction was selected. Therefore, this study opted for silica gel as the buffering material and selected its coefficient of friction at 1.044 under a load mass of 100 g and a speed of 150 mm/min for the analysis of the contact force between the fingertip and the peach.

Table 2   Average static friction coefficient of different materials and navel peach skin

Weight/g	Speed/mm·min⁻¹	Rubber	Expandable polyethylene	Silica gel
100	100	0.743	0.426	1.241
	150	0.706	0.382	1.044
200	100	0.842	0.518	1.328
	150	0.807	0.496	1.287

3.2   Analysis of the mechanical characteristics of peaches

Conducting radial compression tests on peaches at different ripeness stages, Figure 5 depicts a similar curve relationship between compression force and deformation. From the initiation of compression to the onset of yield limit in the peach skin, the relationship between compression force and deformation is approximately linear. After the yield limit, continuing to the rupture of the fruit, the compression force steadily rises to its peak. After the rupture of the fruit, the compression force experiences a sudden decline, and after reaching a certain level, the reduction speed slows down. Table 3 presents the yield limits and displacement of the hardness tester probe for peaches at different ripeness stages. Based on Figure 5 and Table 3, it is evident that fruits at the unripe stage exhibit the maximum yield limit, with an average yield strength of 1.73 MPa. Conversely, fully ripe fruits exhibit the minimum yield limit, with an average yield strength of 0.71 MPa. The compressive strength of peaches decreases with the growth period, indicating that peaches at the green ripe stage are more conducive to storage and transportation whereas fully ripe peaches are better suited for immediate consumption over short distances. Therefore, as long as the force applied by the fingertips of the end-effector during harvesting does not exceed the yield strength of fully ripe fruits, undamaged harvesting of the fruit can be ensured.

According to the engineering materials manual, the elastic modulus E^* of the finger material is 2.7-5.5 MPa. To ensure the reliability of the results, the value of E^*=2.7 MPa was chosen. The effective length was defined as 96% of the actual length of the finger, i.e., l=96 mm. To obtain the minimum value of F, the radius R of the peach was taken as the minimum value of 55 mm. Based on the values of the aforementioned parameters, the calculated value of F was 0.012 N. This is significantly smaller than the experimentally measured yield strength of 0.41 MPa, which is equivalent to 20.09 N (for a probe diameter of 7.9 mm). In other words, the force exerted on the peach through the contact between the fingertips of the harvesting end effector and the fruit is much lower than the yield strength of the peach. This indicates that the grasping force of the fingers has great potential and that the fruit grasping ability of the manipulator is completely feasible. According to a previous analysis,

the adaptive finger adjusts the positive pressure on the fruit based on the different fruit weights to balance the forces on the fruit.
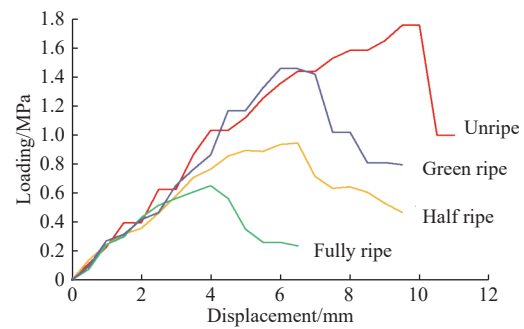

Figure 5   Force–deformation curve of peach under compression

Table 3   Peak rupture force and rupture deformation for peach fruit under compression

Group	Yield limit/MPa			Deformation/mm		
	Max	Min	Avg	Max	Min	Avg
Unripe	1.84	1.45	1.73	8.7	6.3	7.2
Green ripe	1.64	1.07	1.30	6.5	3.8	5.7
Half ripe	1.33	0.82	1.06	7.2	4.3	5.4
Fully ripe	0.87	0.41	0.71	6.5	3.2	4.6

3.3   Physicochemical parameters of the peaches

It can be seen from Table 4 that the two diameters and heights of the peaches were between 60 and 80 mm and that the average value of the three dimensions was about 65 mm. The sphericity range was 0.94-1.08 and the average value was about 1.0. Therefore, it is reasonable to regard peaches as spherical in the mechanical analysis.

Table 4   Statistics of peach shape

Sample	Min	Max	Average	SD
Transverse diameter d_1/mm	60.40	78.00	66.79	3.93
Transverse diameter d_2/mm	55.70	75.90	65.19	4.02
Height h/mm	59.10	71.60	64.57	3.08
Fluid density d_g/mm	59.61	74.45	65.49	3.36
Sphericity Φ/%	0.95	1.08	1.01	0.03
Gravity G/N	1.20	2.27	1.54	0.24

Note: d_1 and d_2 are mutually perpendicular in the equatorial plane of the peach.

Gravity affects the harvesting process. The weight results are listed in Table 4. According to the measurement results, the weight distribution of the peaches was 1.20-2.27 N, and the mean value was 1.54 N. Table 5 lists the values for the range, mean, and standard deviation for the SSCs of the peaches in the different datasets. The samples in each set had adequate variability, and they covered a typical variation range of SSCs. Furthermore, extreme values of the statistical indicators were found in the calibration set for both SSCs. This indicates that more representative samples were assigned to the calibration set. This is undoubtedly beneficial for enhancing the performance of the calibration model.

Table 5   Statistics of the peach soluble solid content

Sample	Number	Soluble solid content/% Brix		
		Minimum	Maximum	Average	SD
Calibration	101	7.47	13.45	11.26	1.061
Validation	34	8.57	13.35	11.27	1.065

3.4   Prediction model and model results

3.4.1   Spectral characteristics and pretreatment effect of peaches

The spectra of 135 peach samples are shown in Figure 6a. There was considerable noise and significant drift in the spectra as

they were affected by multifarious conditions, such as changes in the temperature, diffusion of light, baseline shifting, or instrumental noise, particularly under outdoor conditions. The spectra contained other chemical and physical information that should be taken as noise interference. The shift and drift of the spectral baseline produced light scattering and high-frequency noise, which were caused by the physical characteristics of the peach surface and the changes in the internal cells. SGD, SGS, MSC, and SNV were used to pretreat the NIR spectra. The pretreated spectra are shown in Figure 6b. After pretreatment, the spectra became smooth, and the main absorption peaks were visible, which showed that the treatment effect was good.
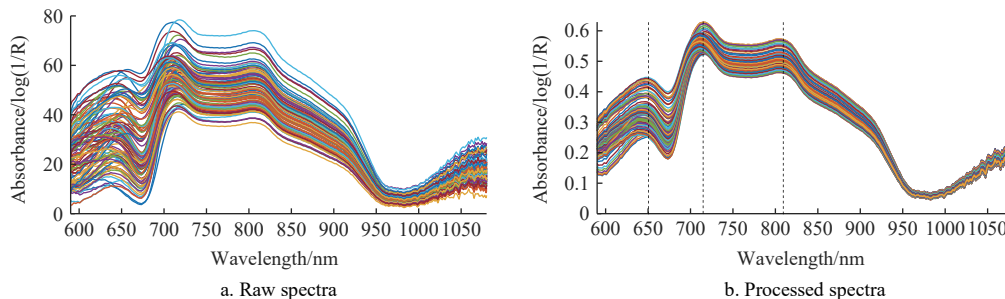

a. Raw spectra   b. Processed spectra

Figure 6   Spectra of peaches: raw spectra and processed spectra

The differences in the visible region were attributed to the color of the peach. There was a higher reflectance peak at 655 nm caused by stronger chlorophyll absorption. The reflectance peak at 710 nm diminished in ripe peaches due to anthocyanin decrease, which was responsible for the red color of the peaches. In the NIR range, the reflectance at around 810 nm was related to the sugar content[35].

3.4.2 Predictive models for the SSC

Models were developed to determine the SSC, as listed in Table 6. For the model established using the raw spectra, the R^2 values of the calibration and the prediction sets were below 0.5. The R^2 value of the model after SGD was about 0.8. The best effect of the model was the spectral modeling after the SGD, SGS, and SNV pretreatment. Because the selected wave band contained visible light, the color information of the sample surface interfered with the model. Therefore, the model substantially improved after the SGD pretreatment. The effect of the SNV and MSC pretreatment on the model was significant, indicating that the spectral differences caused by the physical characteristics of the peach surface were considerable, such as the surface roughness and texture. However, from the effect of the SGS and SGD treatment combined with the SNV and MSC treatments, SNV was better than MSC. The performance of the SGD+SGS+SNV pretreatment model was the best, with determination coefficients R_c^2 and R_v^2 of 0.880 and 0.890 for the calibration and validation sets, respectively, and RMSEC and RMSECV values of 0.370% Brix and 0.357% Brix, respectively. The results of this model were better than those of the effective wavelength selected via the competitive adaptive reweighted sampling and random forest models, with an R_v^2 of 0.88 and an RMSEC of 0.54 for the SSC[30]. Wang et al.[36] generated a regression model for predicting the SSC and firmness of pears via portable visible/NIR spectroscopy, which was obtained using the preprocessing technique coupled with a PLSR model (R^2=0.87). The prediction model showed that the lowest Root Mean Square Error of Prediction (RMSEP) (RMSEP=0.58%) and the highest R_v=0.82 were obtained using six factors employing the processing method by Hemrattrakun et al.[28]. In conclusion, the performance of the model proposed in this study was equivalent to the above research results. Furthermore, the model in this study had a larger R_v^2 value and a smaller RMSECV value, indicating that the model proposed in this study is reasonable.

The results of the verification of the prediction model using the spectra of 30 peaches are shown in Figure 7. The sample points were distributed near the 1:1 trend line. The results indicated that the predicted values of the NIR spectra for the peach SSCs were close to the actual values. These values correlated well with each other. The correlation coefficient for the prediction results and the measured values was 0.936, and the standard error was 0.386% Brix. The above results indicated that the PLSR mathematical model established after pretreatment has practical application value for internal quality identification in the process of peach harvesting.

Table 6   Results of predictive models by PLSR with different pretreatments

Pretreatment method	Factors	R_c^2	RMSEC /% Brix	R_v^2	RMSECV /% Brix
Original spectrum	9	0.373	0.870	0.481	0.785
SGD	12	0.778	0.506	0.798	0.503
SGD+SNV	10	0.879	0.375	0.845	0.435
SGD+MSC	10	0.830	0.442	0.830	0.456
SGD+SGS	11	0.817	0.459	0.836	0.454
SGD+SGS +SNV	13	0.880	0.370	0.890	0.357
SGD+SGS+MSC	10	0.829	0.442	0.828	0.457

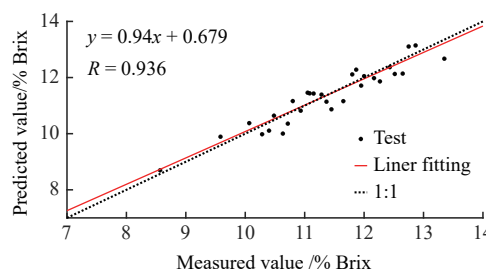Note: PLSR: Partial least squares regression.

Figure 7   Prediction results of peach soluble solids model

4 Conclusions

In this study, an end-effector system for robot harvesting was developed, which was mainly composed of a clamping mechanism, NIR spectrum acquisition system, and control system. The main function of the system was to clamp, collect spectral information, harvest, and grade peaches. The graded harvesting end-effector was designed with adaptive fingers, and a mathematical model was established to analyze the forces of the adaptive fingers on the peach in the harvesting process to ensure that the harvesting end-effector could realize lossless harvesting.

Based on the end-effector system for robot-graded harvesting,

the visible/NIR reflectance spectra of the peaches in the wavelength range of 590-1100 nm were collected. The modeling results of different pretreatment methods indicated that the modeling effect after pretreatment with SGD+SGS+SNV was the best. The R_c^2 and R_v^2 values of the prediction model were 0.880 and 0.890, respectively, and the RMSEC and RMSECV values were 0.370% Brix and 0.357% Brix, respectively. The correlation coefficient for the predicted values of the model and the measured values was 0.936, and the standard error was 0.386. The above data proved the accuracy and robustness of the model. Combined with the graded harvesting end-effector, the NIR nondestructive testing technology of the peach internal quality graded harvesting system could predict the SSCs of the peaches, with good prediction accuracy and stability.

In this study, only the internal quality was utilized as the classification index to prove the feasibility of the graded harvest. In follow-up research, an image acquisition function will be added to the end-effector to analyze the external characteristics of the fruit and to combine various information to judge its quality.

Acknowledgements

[References]

[1]   Yao J H, Chen W J, Fan K. Recent advances in light irradiation for improving the preservation of fruits and vegetables: A review. Food Bioscience, 2023; 56: 103206.

[2]   Jayasooriya L S H, Shin M H, Wijethunga W M U D, Lee S K, Cho J G, Jang S H, et al. Selection of a proper maturity index for the mechanical harvesting of 'Mihong' peach fruit. Horticulturae, 2023; 9(7): 730.

[3]   Hernández-Martínez N R, Blanchard C, Wells D, Salazar-Gutiérrez M R. Current state and future perspectives of commercial strawberry production: A review. Scientia Horticulturae, 2023; 312: 111893.

[4]   Mhamed M, Kabir M H, Zhang Z. Developments of the automated equipment of apple in the orchard: A comprehensive review. In: Towards Unmanned Apple Orchard Production Cycle. Springer, 2023; pp: 1–49.

[5]   Davidson J, Bhusal S, Mo C, Karkee M, Zhang Q. Robotic manipulation for specialty crop harvesting: A review of manipulator and end-effector technologies. Global Journal of Agricultural and Allied Sciences, 2020; 2(1): 25–41.

[6]   Vrochidou E, Tsakalidou V N, Kalathas I, Gkrimpizis T, Pachidis T, Kaburlasos V G. An overview of end effectors in agricultural robotic harvesting systems. Agriculture, 2022; 12(8): 1240.

[7]   Park Y, Seol J, Pak J, Jo Y, Jun J, Son H I. A novel end-effector for a fruit and vegetable harvesting robot: mechanism and field experiment. Precision Agriculture, 2022; 24(3): 948–970.

[8]   Ji W, He G Z, Xu B, Zhang H W, Yu X W. A new picking pattern of a flexible three-fingered end-effector for apple harvesting robot. Agriculture, 2024; 14(1): 102.

[9]   Zhao Y X, Wan X F, Duo H X. Review of rigid fruit and vegetable picking robots. Int J Agric & Biol Eng, 2023; 16(5): 1–11.

[10] Bontsema J, Hemming J, Pekkeriet E, Saeys W, Edan Y, Shapiro A, et al. CROPS: Clever robots for crops. Engineering & Technology Reference, 2015; pp.1–11.

[11] Li Z Y, Yuan X J, Yang Z P. Design, simulation, and experiment for the end effector of a spherical fruit picking robot. International Journal of Advanced Robotic Systems, 2023; 20(6): 1–13.

[12] Li Z, Yuan X, Wang C. A review on structural development and recognition–localization methods for end-effector of fruit-vegetable picking robots. International Journal of Advanced Robotic Systems, 2022;

19(3): 1–29.

[13] Park Y, Seol J, Pak J, Jo Y, Kim C, Son H I. Human-centered approach for an efficient cucumber harvesting robot system: Harvest ordering, visual servoing, and end-effector. Computers and Electronics in Agriculture, 2023; 212: 108116.

[14] Roshanianfard A, Noguchi N. Pumpkin harvesting robotic end-effector. Computers and Electronics in Agriculture, 2020; 174: 105503.

[15] Zhou H Y, Wang X, Au W, Kang H W, Chen C. Intelligent robots for fruit harvesting: Recent developments and future challenges. Precision Agriculture, 2022; 23(5): 1856–1907.

[16] Xiong Y, Peng C, Grimstad L, From P J, Isler V. Development and field evaluation of a strawberry harvesting robot with a cable-driven gripper. Computers and Electronics in Agriculture, 2019; 157: 392–402.

[17] Xu L M, Liu X D, Zhang K L, Xing J J, Yuan Q C, Chen J W, et al. Design and test of end-effector for navel orange picking robot. Transactions of the CSAE, 2018; 34(12): 53–61. (in Chinese)

[18] Mu L T, Cui G P, Liu Y D, Cui Y J, Fu L S, Gejima Y. Design and simulation of an integrated end-effector for picking kiwifruit by robot. Information Processing in Agriculture, 2020; 7(1): 58–71.

[19] Terrile S, Argüelles M, Barrientos A. Comparison of different technologies for soft robotics grippers. Sensors, 2021; 21(9): 3253.

[20] Bhargava A, Bansal A. Quality evaluation of Mono & bi-Colored Apples with computer vision and multispectral imaging. Multimedia Tools and Applications, 2020; 79: 7857–7874.

[21] Bhargava A, Bansal A. Classification and grading of multiple varieties of apple fruit. Food Analytical Methods, 2021; 14(7): 1359–1368.

[22] Bhargava A, Bansal A. Fruits and vegetables quality evaluation using computer vision: A review. Journal of King Saud University - Computer and Information Sciences, 2021; 33(3): 243–257.

[23] Bhargava A, Bansal A. Automatic detection and grading of multiple fruits by machine learning. Food Analytical Methods, 2020; 13(3): 751–761.

[24] Hussein Z, Fawole O A, Opara U L. Harvest and postharvest factors affecting bruise damage of fresh fruits. Horticultural Plant Journal, 2020; 6(1): 1–13.

[25] Dewi T, Risma P, Oktarina Y. Fruit sorting robot based on color and size for an agricultural product packaging system. Bulletin of Electrical Engineering and Informatics, 2020; 9(4): 1438–1445.

[26] Lu Z H, Zhao M F, Luo J, Wang G H, Wang D C. Design of a winter-jujube grading robot based on machine vision. Computers and Electronics in Agriculture, 2021; 186: 106170.

[27] Chen J Q, Qiang H, Wu J H, Xu G W, Wang Z K. Navigation path extraction for greenhouse cucumber-picking robots using the prediction-point Hough transform. Computers and Electronics in Agriculture, 2021; 180: 105911.

[28] Hemrattrakun P, Nakano K, Boonyakiat D, Ohashi S, Maniwara P, Theanjumpol P, et al. Comparison of reflectance and interactance modes of visible and near-infrared spectroscopy for predicting persimmon fruit quality. Food Analytical Methods, 2021; 14: 117–126.

[29] Kusumiyati K, Munawar A A, Suhandy D. Fast, simultaneous and contactless assessment of intact mango fruit by means of near infrared spectroscopy. AIMS Agriculture and Food, 2021; 6(1): 172–184.

[30] Shao Y Y, Wang Y X, Xuan G T. In-field and non-invasive determination of internal quality and ripeness stages of Feicheng peach using a portable hyperspectral imager. Biosystems Engineering, 2021; 212: 115–125.

[31] Goyal R, Kingsly A, Kumar P, Walia H. Physical and mechanical properties of aonla fruits. Journal of Food Engineering, 2007; 82(4): 595–599.

[32] Popov V L. Contact mechanics and friction. Berlin: Springer Berlin Heidelberg, 2010; pp.60–62. doi:10.1007/978-3-642-10803-7.

[33] Sarkar P. Use of shaking mechanism and robotic arm in fruit harvesting: A comprehensive review. Journal of Crop and Weed, 2021; 17(2): 1–9.

[34] Wu X, Li G L, He F Y. Nondestructive analysis of internal quality in pears with a self-made near-infrared spectrum detector combined with multivariate data processing. Foods, 2021; 10(6): 1315.

[35] Zhang H L, Zhan B S, Pan F, Luo W. Determination of soluble solids content in oranges using visible and near infrared full transmittance hyperspectral imaging with comparative analysis of models. Postharvest Biology and Technology, 2020; 163: 111148.

[36] Wang J H, Wang J, Chen Z, Han D H. Development of multi-cultivar models for predicting the soluble solid content and firmness of European pear (Pyrus communis L.) using portable vis-NIR spectroscopy. Postharvest Biology and Technology, 2017; 129: 143–151.